Pulsar: Secure Steganography through Diffusion Models

Tushar M. Jois
City College of New York
tjois@ccny.cuny.edu

Gabrielle Beck
Johns Hopkins University
becgabri@cs.jhu.edu

Gabriel Kaptchuk
Boston University
kaptchuk@bu.edu

Abstract

Widespread efforts to subvert acccess to strong cryptography has renewed interest in steganography, the practice of embedding sensitive messages in mundane cover messages. Recent efforts at provably secure steganography have only focused on text-based generative models and cannot support other types of models, such as diffusion models, which are used for high-quality image synthesis. In this work, we initiate the study of securely embedding steganographic messages into the output of image diffusion models. We identify that the use of variance noise during image generation provides a suitable steganographic channel. We develop our construction, Pulsar, by building optimizations to make this channel practical for communication. Our implementation of Pulsar is capable of embedding $\approx$ 275–542 bytes (on average) into a single image without altering the distribution of the generated image, all in the span of $\approx$ 3 seconds of online time on a laptop. In addition, we discuss how the results of Pulsar can inform future research into diffusion models. Pulsar shows that diffusion models are a promising medium for steganography and censorship resistance.

1 Introduction

Years of sustained effort by the security and cryptography communities has led to widespread deployment of strong, secure communication technologies, including end-to-end encrypted messaging [PM, Wha17] and TLS [Res18]. While these technologies prevent high-resource attackers from viewing or manipulating the contents of communications, they do nothing to hide that the communication itself is occurring. In areas where encrypted communication technologies are blocked or cause for suspicion, leaking this metadata can have deadly consequences. As governments' suspicion of encrypted communication continues to grow around the world, it is important to *proactively* develop new techniques that can complement our existing secure communication technologies and provide security and privacy to individuals at increased risk; if this development is not done proactively, the technology will be too immature for deployment when it is needed.

Steganography [Sim83] allows a sender to embed a sensitive message into a mundane context such that only the intended receiver is able to detect and extract the message, making it the ideal tool for communicating in areas where encryption cannot be safely used. Steganography can be used to transform a conversation that might be seen as "subversive" into one that would not arouse suspicion—even when the content of the conversation itself is directly monitored by authorities. Importantly, this prevents censors from *selectively* blocking content (or selectively blocking encrypted communications). Steganography can also enable digital "dead drop" deployments, in which encoded messages are left on the public internet and the intended recipient can recover the message without leaving evidence of direct communication.

Although the value of efficient, secure steganography tools has been evident for decades, concrete constructions have long been lacking. Formal techniques, stemming from the cryptographic literature, provide provable hiding guarantees but cannot be concretely deployed, either because they are inefficient or make unrealistic assumptions. Heuristic steganographic techniques, on the other hand, have been deployed in practice, but are often vulnerable to simple statistical attacks. For example, JPEG steganography (in which bits of the sensitive message are embedded into the low order bits of pixels' values) is often considered a viable steganographic choice, but the manipulation of low order bits is detectable [FPK07, SCC07].

Steganography for generative models. A new line of research attempts to marry the formal techniques with the heuristic approaches by steganographically encoding messages into the output of generative, machine-learning models. This provides a systematic divide between the provable guarantees and the heuristic assumptions such that they can be analyzed separately. These steganographic schemes can ensure that an adversary cannot distinguish between typical model output and model output carrying a sensitive message, but make no formal claims about an adversary attempting to detect if a message is generated with the help of a model (as opposed to created manually by the sender). While this approach falls short of providing end-to-end security, *this is the best one could hope for* when embedding into contexts where explicit descriptions of the statistical nature of the communication channel cannot be described (e.g. natural human language, art, or photographs). In these cases, encoded messages can only hope to achieve indistinguishably with the best known approximation we have of the communication channel, and machine learning models are the best approximation of natural human language, art, or photographs currently available.

Existing steganographic proposals [KJGR21, DCW+23] are designed to work with popular model structures, like neural networks and general adversarial networks. These models iteratively generate output by producing an explicit probability distribution of different *tokens* (e.g., words, pixels) that could follow the given prompt.

During typical operation, a single token is sampled from this distribution as output, appended to the prompt, and the updated prompt is then fed back into the model. This process continues until the output is the desired length. The randomness used to sample from the distribution is pulled from an arbitrary high entropy source.

When steganographically embedding a sensitive message into the output, the sampling is done as a function of the sensitive message such that the receiver can infer the bits of the sensitive message. For example, the sender might encode the leading bits of the message into a token using an arithmetic encoding scheme or a Huffman code [KJGR21]. To ensure that this steganographic encoding process does not change the statistical profile of the model output, the sensitive message is generally encrypted using a pseudorandom cipher,[1] making it, in effect, a high entropy source.

Steganography for diffusion models. Although text is a natural medium to consider for steganographic communication, embedding into text produces stegotext (the steganography equivalent of ciphertext) that is significantly longer than the initial message. This is because natural language text is actually quite low entropy and steganographic encoding rates are bound by the entropy in the communication channel. As such, sending even relatively short sensitive messages steganographically might require sending paragraphs or pages of model-generated text. While transmitting this much text might occasionally be appropriate, in many cases this will break steganography's illusion. This limitation makes existing, text-based approaches insufficient, motivating the need for encoding techniques that work with other media.

After text, images are the next media into which we might want to embed steganographic messages. Importantly, images do not share the same limitations as text: images have significantly higher entropy than text and it is commonplace to exchange or post large image files. These properties mean that it should (in principle) be possible to steganographically send large amounts of information using machine learning-generated images without arousing suspicion. Building on this intuition, Ding et al. [DCW+23] generated steganographic images using ImageGPT, a neural network designed to produce images based on a prompt.

While transformer networks remain the most effective generative models in the natural language processing domain, a new model architecture, *diffusion models* [SDWMG15, SME20, HJA20, DN21, RBL+22], have proven to produce higher quality output for images. Diffusion models have quickly captured the public's imagination and have become the *de facto* option for machine-learning image generation. Unlike neural networks, diffusion models generate all the pixels in the output image at the same time. This significant departure from typical transformer network architecture means that existing steganographic approaches cannot be adapted to efficiently work for diffusion models.

In this work, we initiate the study of steganographic embedding mechanisms that can work with diffusion models. Our techniques allow for the production of steganographic communication tools that can send large

[1] Some proposals [GGA+05, SSSS07, YHC+09, CC10, CC14, FJA17, VNBB17, YJH+18, Xia18, YGC+19, HH19, DC19, ZDR19] fail to properly encrypt the message before encoding, leading to an insecure construction.

amounts of data without arousing suspicion. Additionally, we find that encoding with diffusion models can be *faster* than encoding with other networks, because encoding using existing techniques requires querying a transformer model many times while diffusion models are *one shot*. Additionally, the justification for using machine learning models in steganography relies on the assumption that the models are the best available approximation of human creation. Using other models in steganographic image generation undermines this assumption, as diffusion models have surpassed their quality.

Our contributions. We initiate the study of steganographic encoding schemes for images generated by diffusion models. In doing so, we have several concrete contributions:

- **A principled study of steganography for diffusion models.** As we are initiating the study of steganographic for diffusion models, we begin our work by providing a principled study of the various opportunities for hiding data that diffusion models afford. We begin by noting that cryptographically secure steganography is fundamentally about *randomness recovery*. As such, we can systematically iterate through the entropy sources consumed by a machine learning model and identify those that are most promising for hiding data. This study ensures that our construction, Pulsar, is optimized to encode as much data as possible.

- **Pulsar, a novel steganographic encoding scheme for diffusion models.** We design a novel, symmetric key steganographic encoding scheme that encodes data into the output of diffusion models that operate in the pixel space.[2] Pulsar embeds data into images by mapping pixels in the image to bits in the message; when sampling Gaussian noise for each pixel, the encoder uses one of two pseudorandom functions, one for pixels mapped to a zero bit and one for pixels mapped to a one bit. This results in a noisy, randomness recovery scheme, which can be improved using error correcting codes. We implement Pulsar and integrate it with existing diffusion models, showing that it can encode hundreds of bytes of plaintext information in a 256×256 pixel generated image. Our implementation encodes faster than state-of-the-art neural network steganographic systems.

- **Recommendations for steganography-friendly machine learning models.** We note that the empirical nature of machine learning research can lead to some model architectures incorporating semi-arbitrary design choices, while also significantly impairing the ability to steganographically embed messages into model output. Reflecting on our study of steganography for diffusion models, we highlight several ways in which model architecture can be improved to better support steganographic encoding. We hope that this can inspire designers of future model architectures to test if models can be made steganography friendly without reducing output quality.

Deployment scenario and threat model. In this work we assume a similar deployment scenario and threat model as recent work on symmetric key, model-based steganography [KJGR21, DCW$^+$23]. Namely, a sender and receiver generate shared key material out-of-band and select a diffusion model to use as a covert channel. We assume that their communications are monitored by a computationally powerful adversary (e.g., a state actor) who also has access to the selected diffusion model. The sender and receiver wish to disguise the contents of their communication such that the adversary cannot determine if their exchanged messages contain typical model output or steganographically encoded messages. As this work focuses of laying out a feasibility result, we make the simplifying assumption that the adversary does not launch active attacks and must distinguish based on observing encoded messages.

We do not attempt to formalize the ability of the adversary to distinguish between model output and "normal" human communication. For full-scale deployments of steganography, deployment designers must carefully consider how well steganographically generated messages fit in with existing communication channels (in addition to incorporating other best practices from cryptographic messaging like forward security). While this is certainly a limitation of our work, we note that humans exchanging the outputs of generative

[2] Pulsar is designed for models that operate in the pixel space, as opposed to a compressed latent space. We discuss this difference in Section 3.1

models has become increasingly common. For example, professional communications may be generated with the help of text models like ChatGPT [Kor23] and social media was flooded with "AI art" [Vin22] after the release of Stable Diffusion [RBL+22] and similar models. These developments mitigate the risks associated with encoding information in model output.

2 Related Work

Steganography maps a message into a stegotext, a set of elements from a chosen target distribution. Typically, this distribution is mundane such that a censor would not find it suspicious. This strengthens encryption, in which a ciphertext can have an arbitrary distribution and does not aim to hid the fact that it is a ciphertext.

Steganography was first formalized by Simmons [Sim83] and has since been the subject of a tremendous amount of theoretical research. The theoretical literature has focused on establishing the universal feasibility of steganography for arbitrary stegotext distributions, provided the distribution has some amount of entropy. For example, prior work has shown that universal steganography can be realized with information-theoretic security [AP98, ZFK+98, Mit99, Cac00], computational security, [HLv02, vH04, BC05] and statistical security [SSM+06a, SSM07, SSM+06b]. There are also symmetric-key [Cac00, HLv02, RR03] and public-key constructions [vH04, BC05, Le03, LK03] discussed in the literature. More recently, techniques deeply related to steganography have been studied as a tool to achieve security when an adversary is able to compel a receiver to decrypt ciphertexts [HPRV19, PPY22].

A complementary line of research has studied the feasibility of concretely efficient, deployable steganography. Generally, to achieve this result, these steganographic constructions either rely on heuristic security analyses, e.g., protocol obfuscators like obfs4/ScrambleSuit [WPF13] and domain fronting [FLH+15], or can only embed messages into very specific covertext distributions, e.g., pseudorandom bit streams. For example, SkypeMorph [MLDG12], CensorProofer [WGN+12], and FreeWave [HRBS13] all tunnel Tor [RSG98, DMS04, Tor] traffic through Voice-Over-IP (VoIP) traffic, which is usually encrypted with a pseudorandom cipher. Other examples include Format Transforming Encryption [LDJ+14, DCRS13, DCS15, OYZ+20], which requires implementers to explicitly describe the statistical properties of the target distribution.

Recently, there has also been work attempting to leverage generative neural networks to instantiate concretely efficient universal steganography by embedding messages into the output of the model. By using machine learning models, these works cleanly separate their heuristic guarantees from their formal ones. Specifically, these protocols offer no formal guarantees about how easy it is to detect that content has been produced by a machine learning model, but can make formal arguments about the statistical shifts induced by the steganographic embedding. This line of work started in the machine learning community with constructions that modified the output distribution of the model, thus falling short of any notion of provable security [Bal17, HWJ+18, Har18, SAZ+18, Cha19, WYL18]. Building on these works, Kaptchuk et al. [KJGR21] and Ding et al. [DCW+23] showed how to encode steganography messages into neural network output without modifying the output distribution. Kaptchuk et al. [KJGR21] accomplish this by repeatedly re-encrypting the message using a stream cipher, using the resulting pseudorandom ciphertext bits to sample tokens from the neural network's probability distribution, and leveraging an arithmetic encoding scheme to enable a receiver to recover the message bits. Ding et al. [DCW+23] are able to achieve a better encoding rate by using the message bits to "rotate" the neural network's probability distribution before sampling. As we discuss in the next section, the techniques presented in these works cannot be adapted to work with diffusion models, as they make implicit assumptions about the model architecture of generative models that do not hold for diffusion models.

3 Steganography for Diffusion Models

We start by systematically exploring the opportunities that diffusion models provide for steganographic encoding.

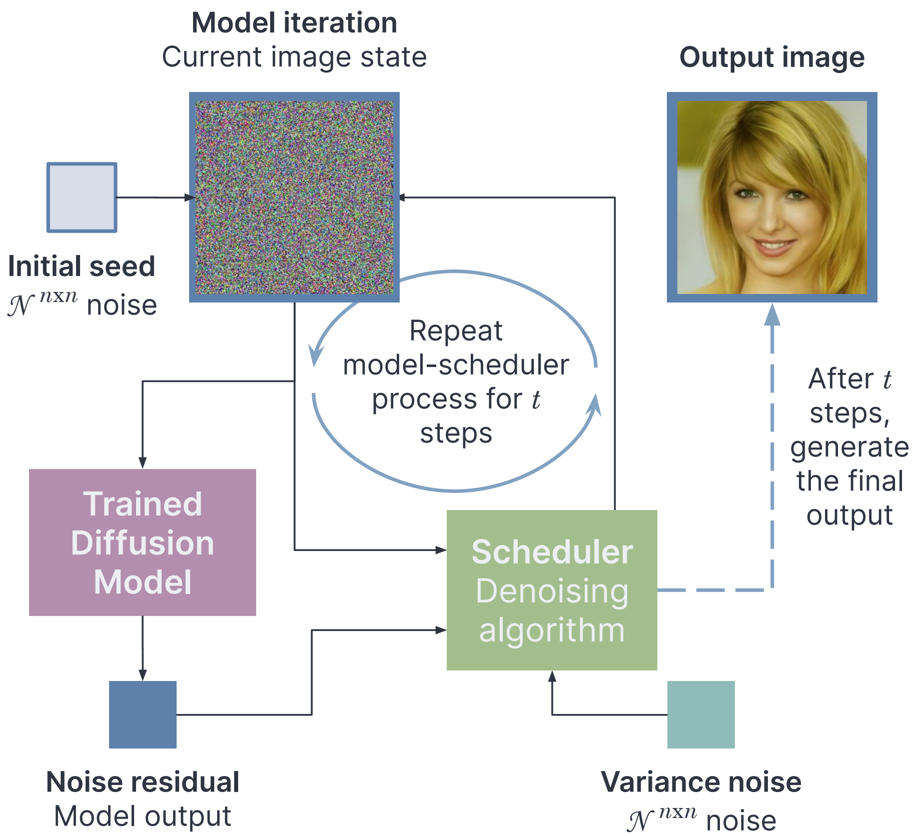

Figure 1: An overview of inference in a diffusion model. The model-scheduler feedback loop continues for all t steps of the scheduler, after which the final image is output.

3.1 Diffusion Models

Diffusion models [SDWMG15, SME20, HJA20, DN21, RBL+22] are a novel generative model architecture tailored to produce visual media. Rather than generate output one token at a time, as is common in the neural networks used in language models, diffusion models take in a random seed (and possibly a prompt) and produce the entire image at once. The model predicts the changes that would need to be applied to this seed to make the image closer to the desired distribution, e.g., photo-realistic images or fantasy art. We provide a visual representation of the generation process for a typical diffusion model in Figure 1.

Diffusion models are trained on a large corpus of training examples. Each example is a pair of images $(\mathsf{img}, \mathsf{img} + \mathcal{N}(0, I))$, where img is an image from the desired output distribution and $\mathsf{img} + \mathcal{N}(0, I)$ is a modified version of img with Gaussian noise added. Many examples are created from each img, with multiple values of I; the most extreme examples appear to be pure noise while others are quite close to the output image. Given these examples (along with the value of I), the model is trained to predict a value from $\mathcal{N}(0, I)$ such that it can be subtracted from the example to recover img.

During image generation (Algorithm 1), the pipeline is reversed: a seed s_0 is sampled from a Gaussian distribution, and the model predicts a *noise residual* pred such that $s_0 - \mathsf{pred}$ is in the target distribution. Rather than remove pred all at once, the model takes pred as an indication of the *direction* in which it must modify the s_0 to get it to the desired distribution. As such, the model subtracts a function of pred rather than pred itself. For example, the models that we work with compute $s_1 = s_0 - \epsilon \cdot \mathsf{pred}$, for some $0 < \epsilon < 1$. This process is repeated a fixed number of times to produce the values $s_2, \ldots, s_{\mathsf{final}}$; recall that the model

Algorithm 1: Typical Diffusion Model Operation

Output: Generated Image img

Set $s_0 \xleftarrow{\$} \mathcal{N}^{n\times n}$

for $1 \le i < t$ **do**

  $r_i \xleftarrow{\$} \mathcal{N}^{n\times n}$

  $\mathsf{pred}_i \leftarrow \mathsf{Model}(s_{i-1})$

  $s_i \leftarrow \mathsf{Scheduler}_i(s_{i-1}, \mathsf{pred}_i; r_i)$

`// Deterministic Final Schedule`

$\mathsf{pred}_t \leftarrow \mathsf{Model}(s_{t-1})$

$\mathsf{img} \leftarrow \mathsf{Scheduler}_{\mathsf{final}}(s_{t-1}, \mathsf{pred}_t)$

Output img

Figure 2: Typical diffusion model image generation

was trained on many levels of noised images and can predict the noise that should be removed from $s_1, s_2, \ldots$ even though they are "less noisy" than s_0.

This iterative process is called *denoising* [SME20, HJA20] and is organized according to a *schedule*, which we denote with a set of functions $\{\mathsf{Scheduler}_i\}_{i\in[t]}$. Each function determines *how* the prediction from the model should be applied to the state s_{i-1} to produce an updated state s_i (e.g. applying the ϵ scaling factor). Different concrete instantiations of diffusion models also might incorporate different modifications into each step of the schedule. One common modification is to apply additional Gaussian noise, called *variance noise*, to s_i in each step $i < t$, ensuring that image generation is *non-deterministic*. The final image is then generated deterministically by $\mathsf{Scheduler}_t$.

In the above, we have described the diffusion process as though the seed s_0 and intermediary states $s_1, s_2, \ldots$ are all elements in the image space (i.e., if the model is trained to generate 256×256 color images, then s_i is also a 256×256 color image). In practice, the space of s_i can be different than the image space; some diffusion models (e.g. Stable Diffusion [RBL+22]) operate in a latent space, a compressed space that is more succinctly able to represent and capture the complexity of images. When operating in the latent space, the model adds a final mapping step that maps s_{final} into a final image using a variational autoencoder (VAE) [KW13].

3.2 Integrating Steganography

Given the structure of diffusion models, we can now turn to the task of studying the steganographic opportunities that structure affords. We first discuss why existing steganographic techniques cannot be directly adapted to work with this model structure. Next, we review classical steganographic techniques before turning to the opportunities themselves.

Why existing techniques fall short. A natural approach to steganography for diffusion models would be to extract the intuition behind steganographic approaches designed for other machine learning model architectures and adapt it for this new architecture. For example, Meteor [KJGR21] and Discop [DCW+23] are steganographic approaches for transformer-like architectures, which are the leading models for text generation. Both follow the same template: given some initial prompt (representing the context in which the encoded message will be sent) the sender uses the machine learning model to produce an explicit probability distribution over the token (e.g., a word) to be appended to the prompt. During typical generation, neural-network-like architectures would select a token from this probability distribution at random. When encoding a message steganographically, both constructions instead sample the token as a function of the message.[3] Importantly, the receiver can use knowledge of the probability distribution and the selected token to efficiently

[3] Meteor encrypts the message first, to ensure the message is uniformly distributed. Discop instead uses an information theoretically secure approach to selecting the token, and thus does not require encryption.

recover a few bits of the message (in both cases, the receiver can recover a variable number of bits). The sender can repeat this process, appending samples to the prompt until the entire message is encoded.

Critical to the approaches of Meteor and Discop is the assumption that the receiver gets access to the results of many (conditionally linked) sampling events. Although it is theoretically possible for a token to encode a large number of bits, the chances of this happening become vanishingly small as the number of bits increases. The throughput of the steganographic encoding scheme is tightly linked to the entropy in the channel: the expected number of bits to encode cannot exceed the instantaneous entropy in the model output distribution. For example, if a message is 128 bits long, it could only be encoded into a single token if the chances of choosing that token were 2^{-128} (assuming the sender and receiver share no prior information about the message distribution).

The structure required by Meteor and Discop is not present in diffusion models. Specifically, diffusion models do not produce explicit probability distributions from which the image is sampled. Moreover, the entire output that is accessible to the receiver is produced in a single shot, making subdivision (e.g., encoding into each pixel independently) impossible. Even adapting more classical steganographic schemes to diffusion models seems challenging. For example, foundational steganographic constructions (e.g. [Cac00, HLv02, vH04]) rely on the use of universal hash functions to subdivide the output space into segments that correspond to different bit sequences and then use rejection sampling to find a sample output that hashes to the desired message. While it is possible to use such a technique with diffusion models, the entire message would need to be encoded into the singular output image. Even though an image might be high entropy enough to encode a large number of bits, using rejection sampling to find an image that hashes to the desired bits is computationally infeasible.

Opportunities for steganography. While there are numerous techniques that can be used to construct steganography, all of them rely on embedding the message into the entropy in the channel. Because the space of messages that can be sent over a particular communication channel is fixed by the distribution within which the encoded message is supposed to hide, the *choice* of which message to send is the only subliminal channel available. Therefore, when evaluating the opportunities for steganographically embedding into the output of diffusion models, we begin by examining the sources of entropy.

When generating images, diffusion models use two sources of entropy: (1) the initialization seed, and (2) the noise added during each step of the schedule. To understand the viability of using these sources, we must understand how using different randomness for each changes the image seen by the receiver. We study this question *empirically*, as randomness is largely a means to an end within these models.

1. *Initialization seed:* It is tempting to try and embed the message into the initialization seed used by the model. Because this seed is both large and high entropy, it is natural to assume that we could steganographically embed a large amount of information into the seed. Unfortunately the image generation process is not invertible. In our experiments with real-world diffusion models, we found that each step of the scheduler was injective, but not surjective. Even if only some information was lost in each step of the scheduler, most concrete instantiations of diffusion models have as many as 50 steps, each one of which is unpredictably lossy. As such, it is unclear how to steganographically embed information into the seed while allowing it to be recoverable.

2. *Variance noise added by scheduler:* Each step of the schedule adds a small amount of Gaussian noise to the current state s_i. In our experiments, we found that modifying the noise added to a single pixel in state s_i can result in a small, local change in the equivalent pixel in s_{i+1}. When operating in the latent space, the decompression results in changes not only in the equivalent point in the latent space, but also to surrounding points; this effect is amplified when the resulting latent space is mapped into the image space.

The localized nature of (2) provides an opportunity for an efficient steganographic channel, which we investigate below.

(a) A Pulsar reference image img_0.

(b) A Pulsar reference image img_1.

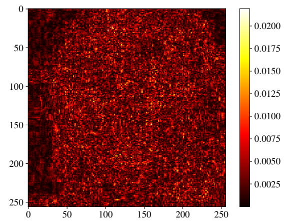

(c) The difference heatmap representing the magnitude of the differences between Figures 3a and 3b.

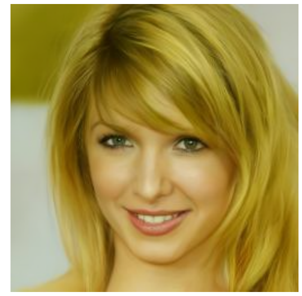

(d) A Pulsar image which encodes 620 bytes.

Figure 3: Sample output from the `celebahq` model. Note that the differences shown in (c) are not changes introduced to encode a message, but a reflection of the entropy in the generative model that we exploit to embed steganographically.

4 Pulsar: A Symmetric Key Steganographic Scheme for Diffusion Models

We now describe Pulsar, a symmetric-key steganographic encoding scheme for pixel-space diffusion models.

4.1 Intuition

Pulsar leverages the steganographic channel enabled by the addition of Gaussian noise in the schedule. As discussed above, resampling the noise for a pixel in the final round of the schedule can result in localized change to the output image. When this resampling is a function of the message, the receiver can observe these changes and recover the message.

In more detail, the sender and receiver share key material that allows them to derandomize their model operation such that they can keep their models perfectly synchronized. This allows the sender and receiver to have their models generate the same exact image. We divide this key material into three concrete PRG keys: a *seed* key k_s, and then a pair of *reference image* keys k_0 and k_1. The seed key is used by both the sender and receiver to synchronize their models until the final step of the scheduler, i.e. they use k_s to sample the model's initial seed and sample the variance noise in the first $t-1$ scheduler iterations. The sender and receiver can then generate two reference images $\mathsf{img}_0, \mathsf{img}_1$ by sampling the variance noise for the t^{th} iteration of the sampler with k_0 and k_1 respectively. To illustrate this process, we include concrete reference images img_0 and img_1 in Figures 3a and 3b.

In order to build intuition, we make the following simplifying assumptions: (1) the model's state is simply the pixels of the image itself, and (2) the final iteration of the scheduler operates on each element of the state independently, i.e., each element of the final state is a function of exactly the corresponding element in the previous state and neighboring elements have no effect on one another. If these assumptions were true, a clear steganographic channel would emerge. The sender would divide the message m they want to send into bits $m_0, m_1, \ldots$ and then sample variance noise for each element of the state from k_0 or k_1 depending on the bit value of the message. For example, if message bit m_i were b, then the sender samples the variance noise for the i^{th} element using k_b. The receiver can then *guess* about the value of m_i by comparing the final output of the model to img_0 and img_1; whichever reference image the final output more closely resembles in the i^{th} pixel determine the receivers guess about m_i. This would allow the sender and receiver to encode a single bit per pixel.

These simplifying assumptions serve a unified purpose: minimizing the error rate in the channel. Indeed, even without these assumptions, there may *still* be errors, as the reference images may be identical in particular pixels. For example, see Figure 3c, in which we give a heatmap of the difference between the

Algorithm 2: Pulsar Encode

Input: Plaintext Message m, Key k

Output: Stegotext Image img

```
Parse (k_s, k_0, k_1) ← k                                   // Offline Phase
Set s_0 ←$ N_{k_s}^{n×n}
for 1 ≤ i < t − 1 do
    r_i ←$ N_{k_s}^{n×n}
    pred_i ← Model(s_{i−1})
    s_i ← Scheduler_i(s_{i−1}; r_i)
Compute rate ← EstimateRate(s_{t−2})
m_ECC ← ECC.Encode(m, rate)                                 // Online Phase
for 0 ≤ j < |m_ECC| do
    if m_ECC[j] = 0 then
        r_{t−1}[j] ←$ N_{k_0}
    else
        r_{t−1}[j] ←$ N_{k_1}
pred_{t−1} ← Model(s_{t−2})
s_{t−1} ← Scheduler_{t−1}(s_{t−2}, pred_{t−1}; r_{t−1})
// Deterministic Final Schedule
pred_t ← Model(s_{t−1})
img ← Scheduler_t(s_{t−1}, pred_t)
Output img
```

Figure 4: Pulsar Encode

two example reference images. Black pixels in this heatmap show that resampling the Gaussian noise has negligible effect on the final pixel value. Without assumption (2), sampling variance noise from different sources might have unpredictable effects, as the changes to one particular pixel might "contaminate" the signal in neighboring pixels. Finally, if the state does not have a clean correspondence to the image, it may not be clear where the receiver should look to recover information about how variance noise is sampled.

To recover from these errors, we introduce the use of a *binary error correcting code*. A binary error correcting code introduces redundancy into a message such that when the message is transmitted over a noisy channel (i.e., a channel that introduces bit flips), the receiver can run some recovery algorithm and output the initial message. Careful use of this error correcting code allows us to continue using the same intuition above, but ensures that the message can be recovered from the receiver, even without our simplifying assumptions.

We begin by removing assumption (2) and accept that changes in the way variance of noise is sampled for a particular pixel may impact neighboring pixels—or, indeed, any pixel; we simply treat this as additional error to be corrected. The sender and receiver synchronize their models as before, reaching the final iteration of the scheduler. Before attempting to encode the message, the sender first encodes the message with a binary error correcting code, and then proceeds as before. Only one question remains: what *rate* should the sender use for their error correcting code, i.e., how *much* redundancy should the sender add into the message. If the error rate is high, the sender needs to increase the redundancy, as more information will be erased by the channel. On the other hand, adding unnecessary redundancy is wasteful, as fewer message bits will fit in the fixed capacity of the image.

To fix the rate of the error correcting code, the sender *estimates* the error rate. While it might be possible to use a fixed error rate, our experiments found that different images have very different error rates that are

Algorithm 3: Pulsar Decode

Input: Stegotext Image img, Key k

Output: Plaintext Message m

Parse $(k_s, k_0, k_1) \leftarrow k$ `// Offline Phase`

Set $s_0 \xleftarrow{\$} \mathcal{N}_{k_s}^{n\times n}$

for $1 \le i < t-1$ **do**

  $r_i \xleftarrow{\$} \mathcal{N}_{k_s}^{n\times n}$

  $\mathsf{pred}_i \leftarrow \mathsf{Model}(s_{i-1})$

  $s_i \leftarrow \mathsf{Scheduler}_i(s_{i-1}; r_i)$

Compute $\mathsf{rate} \leftarrow \mathsf{EstimateRate}(s_{t-2})$

$\mathsf{pred}_{t-1} \leftarrow \mathsf{Model}(s_{t-2})$

`// Generate reference image 0`

Set $r^0_{t-1} \xleftarrow{\$} \mathcal{N}_{k_0}^{n\times n}$

Set $s^0_{t-1} \leftarrow \mathsf{Scheduler}_{t-1}(s_{t-2}, \mathsf{pred}_{t-1}; r^0_{t-1})$

$\mathsf{pred}^0_t \leftarrow \mathsf{Model}(s^0_{t-1})$

$\mathsf{img}_0 \leftarrow \mathsf{Scheduler}_t(s^0_{t-1}, \mathsf{pred}^0_t)$

`// Generate reference image 1`

$r^1_{t-1} \xleftarrow{\$} \mathcal{N}_{k_1}^{n\times n}$

Set $s^1_{t-1} \leftarrow \mathsf{Scheduler}_{t-1}(s_{t-2}, \mathsf{pred}_{t-1}; r^1_{t-1})$

$\mathsf{pred}^1_t \leftarrow \mathsf{Model}(s^1_{t-1})$

$\mathsf{img}_1 \leftarrow \mathsf{Scheduler}_t(s^1_{t-1}, \mathsf{pred}^1_t)$

for $0 \le j < |m_{\mathsf{ECC}}|$ **do** `// Online Phase`

  if $|\mathsf{img}[j] - \mathsf{img}_0[j]| < |\mathsf{img}[j] - \mathsf{img}_1[j]|$ **then**

    $m_{\mathsf{ECC}}[j] \leftarrow 0$

  else

    $m_{\mathsf{ECC}}[j] \leftarrow 1$

Output $m \leftarrow \mathsf{ECC.Recover}(m_{\mathsf{ECC}}, \mathsf{rate})$

Figure 5: Pulsar Decode

dependent on the structure of the image (discussed more in Section 5). As such, we instead have the sender estimate the error rate for each generated image by encoding random messages into the last iteration of the scheduler and measuring the number of errors by attempting to recover the encoded message. This process allows the sender to get a good estimate on the error rate, and then use conservative parameters on the error correcting code to ensure recovering the message is possible with high probability.

Relaxing assumption (1) appears to be more challenging. As discussed above, many concrete instantiations of diffusion models (e.g., Stable Diffusion) operate on a *latent space*, a compressed representation of the pixel space, in order to be more efficient. This design choice necessitates the use of an expanding mapping between the latent space and the pixel space. While we find that the approach outlined above can function for such models, the result is highly inefficient. As such, we restrict attention to diffusion models that operate directly in the pixel space. We included a more detailed discussion of diffusion models in the latent space in Section 7.

4.2 Pulsar Description

Notation. We assume that the sender and receiver (and adversary) both have access to the same diffusion model that operates in the pixel space and generates $n \times n$ pixel images[4] with 3 color channels, resulting in a image space of $[0, 255]^{n \times n \times 3}$. Let this diffusion model have an associated scheduler $\mathsf{Scheduler} : [0, 255]^{n \times n \times 3} \times \mathbb{Z} \rightarrow [0, 255]^{n \times n \times 3}$. Let $\mathcal{N}(0, I)$ be a Gaussian, and $\mathcal{N}^{n \times n}(0, I)$ be $n \times n$ copies of the underlying Gaussian. We denote a *keyed* Gaussian as $\mathcal{N}_k(0, I)$, in that samples drawn from the Gaussian are drawn using entropy generated by a pseudorandom generator [BM82, Ruh17] with key k. As the norm and standard deviation of the distribution are fixed model parameters, we omit them. We abuse notation and write $s + \mathcal{N}$ to denote sampling a value from $\mathcal{N}$ before adding it to s.

We index into images and messages using square bracket notation, i.e., $x[i]$ is the i^{th} element x. For images, we assume some arbitrary pixel ordering to facilitate single dimension indexing. Let ECC be an error correcting code made up of two algorithms: and encoding algorithm ECC.Encode and a recovery algorithm ECC.Recover. Both take in a message and an error rate. We expand on error correcting codes and the properties we require of them in Section 5.

Pulsar encoding and decoding. The encode and decode algorithms for Pulsar are described in Algorithm 2 and Algorithm 3 respectively. When encoding, the sender runs the typical image generation algorithm for the first $t - 2$ iterations. The sender then estimates the error rate for encoding and adds redundancy to the message using an error correcting code ECC. Then, based on the bits of the expanded message m_{ECC}, the sender samples variance noise either using k_0 or k_1. Then, the final image is generated using $\mathsf{Scheduler}_t$. When decoding, the receiver estimates the error rate in the image and generates reference images img_0 and img_1. In order to recover m_{ECC}, the receiver compares each pixel to the reference images, and guesses the corresponding bit of m_{ECC} accordingly. m can then be recovered by applying ECC.Recover.

Offline-online paradigm. We note that much of the logic of Pulsar can be run before the sender knows the message. Specifically, the first $t - 2$ iterations of the schedule are completely independent of the message. As such, this computation can be run *offline*, and the results can be stored until the sender has a message they want to encode. At that time, the sender can run the *online* parts of Pulsar, which include ECC, sampling the variance noise r_{t-1}, and final image generation. We highlight the offline and online phases of encoding and decoding in Algorithm 2 and Algorithm 3.

Proof sketch. To show security, we consider a real-or-random notion of chosen hidden-text security, similar to in Meteor [KJGR21], in which the adversary must distinguish if it gets access to a typical model generation oracle or a steganographic encoding oracle. The security of Pulsar is a straightforward reduction to the security of the pseudorandom generator used to sample Gaussian noise. Informally, a computationally bounded adversary can not distinguish between real randomness and the pseudorandomness output by the PRG. As such, the adversary cannot distinguish between variance noise that is honestly sampled and that is sampled from different PRGs. The proof is simply a set of hybrids in which each sampling event when embedding m_{ECC} is swapped from true randomness to the appropriate PRG. The final hybrid derandomizes the first $t - 2$ iterations of the schedule, swapping honest randomness for pseudorandomness generated using k_s.

5 Error Correction for Pulsar

We now investigate how to build EstimateRate and select an ECC for Pulsar to maximize throughput.

5.1 Channel Error Structure

A naive approach to computing EstimateRate would simply have the sender generate a random message, encode it into an image, locally attempt to recover it and measure the decoding error rate. Based on this

[4] We assume square images for simplicity, but other dimensions are trivially supported.

error rate, they would select an ECC that can successfully encode at that error rate. For instance, an estimate for the error rate of the image in Figure 3d is high (29.1%) but we can build a code for this high error rate.

To improve on this baseline, we investigate the sources of error a little more closely. An error occurs in Pulsar when, for a bit b, the difference in the corresponding pixel between the encoded img and $\mathsf{img}_{b'}$ is closer than that of img and img_b, where $b \neq b'$. There is, therefore, a inverse relationship between the absolute *magnitude* of differences between the references images img_0 and img_1 and the error rate: roughly speaking, the greater the difference for a pixel, the less likely decoding that pixel will result in an error. The naive approach above assumes that the distribution of errors is uniform throughout the image.

A closer look at the heatmap in Figure 3c reveals that the differences between img_0 and img_1 are not uniformly distributed in the image—there is structure. The heatmap is dark for the regions of the image that make up the background in Figure 3d, creating a semi-visible silhouette of the face. In this significant background region, the differences between img_0 and img_1 are consistently low. Because Pulsar leverages differences in order to steganographically embed, the background will contribute more to the error rate than the rest of the image. Put another way, any single bit encoded in this part of the image will have a much higher error rate.

This notion of "difference regions" with varying magnitudes is more obvious when looking at Figure 6a and associated heatmap in Figure 6b. In addition to the background, parts of the generated face are also less discernible, and the estimated overall error rate is 34.1%: over one in three bits is incorrectly decoded. Not only are there distinct difference regions, but they also differ from image to image.

5.2 Variable Error Correction

The naive approach in Section 5.1 fails to fully utilize the high entropy present in some regions of the image. The model is more detailed in some areas, leading to high entropy (and low error). In other areas, the model is less detailed, and so the available entropy is lower. These regions are essentially *guaranteed* to introduce high amounts of error, diluting the overall error rate. Unlike most applications of error correcting codes, however, in Pulsar we actually *can* estimate where the errors will happen; we can divide the communication channel into smaller channels, each of which has a predictable error rate.

An obvious solution would be to leverage the sender's and receiver's shared knowledge of the image structure to *only* encode into those regions that contain low error rates. This would entail selecting a code for low error regimes and using that on these regions. This approach would work, but is also inefficient. The number of low error regions is image-dependent; an image like Figure 3d has many more than an image like Figure 6a. Additionally, this approach excludes "medium" error rate regions, i.e., where the error rate is between low and high. These regions will have relatively higher error rates, but could still encode *some* amount of data.

So, what we need is a *library* of error correcting codes, selecting the best code for a region based on its error rate. Intuitively, if we can define these difference regions, we can estimate the error rates within each region separately, and then select error correcting codes per-region instead of over the image overall. This approach helps us more efficiently utilize the low error rate regions of the image to encode bytes.

Our region-based error rate estimation for EstimateRate proceeds as follows. First, we use the naive error estimate strategy on each difference region of the image individually. To do so, we compute l trial encodings at the current model state on random messages. These trail encodings are then subsequently decoded to generate difference heatmaps (like those seen in Figures 3c and 6b). To systematically define the difference regions from these heatmaps, we divide the pixels in the image into u buckets based on the magnitude of the difference shown in the heatmap. Each bucket represents one unique difference region of the image—all of the pixels in a bucket have a similar magnitude of their differences and therefore (roughly) similar error rates during Pulsar encoding. We chose to bucketize the differences rather than apply image analysis (e.g., convolution to find region boundaries) because the latter would involve more expensive techniques and may miss difference regions that are non-contiguous.

We calculate the error rate for each difference regions, as defined by its bucket, based on the messages from the trial encoding. rate is now a list of regions with associated error rates, we select the appropriate ECC for each region. To do so, we start with the lowest error regions, and use codes suitable for those

(a) A Pulsar image which encodes 200 bytes.

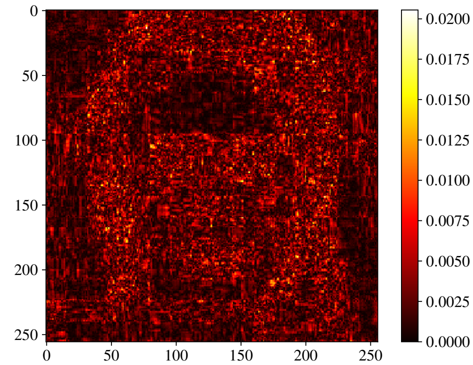

(b) The difference heatmap for the img_0 and img_1 used to create Figure 6a.

Figure 6: Another sample output for the `celebahq` model.

regions. We then work our way up the difference regions, selecting a code from our library that works at each region's calculated error rate. Eventually, we reach a region that cannot be encoded using our codes due to its significant noise, and we consider encoding finished.

Using this approach, Figure 3d can encode 620 bytes of information, and Figure 6a can encode 200 bytes of information. We also note that EstimateRate is still a fully offline operation (Section 4.2), as the difference regions for an image can be estimated without any information about the message to encode. Both the sender and receiver can perform multiple runs of EstimateRate in preparation for a communication.

Note that our EstimateRate has two parameters: the number of buckets for each estimate u, and the number of estimates l. We experimentally determine these parameters, and present our results in Section 6.1. A more formal description of EstimateRate can be found in Appendix A.

5.3 Identifying Candidate Codes

Our variable error correction approach requires building a library of error correcting codes that support differing error rates, such that more efficient codes can be used in difference regions with low error. We approach the development of this library *heuristically*, as developing optimal codes for our setting is a difficult problem beyond the scope of this work. We note, however, that there may be significant room for Pulsar performance improvement by identifying superior codes.

Error correcting codes. In this work we will consider linear $[N, k, d]_q$ codes, which are codes defined over a field $\mathbb{F}_q$ of size q. The size of the codeword N is called the *block length*, k is the *dimension* and d is the *distance* of the code. The *rate* of a code is given by $\frac{k}{N}$ and the unique decoding radius (the number of errors a code can tolerate while still uniquely recovering the original codeword) is $\lfloor \frac{d}{2} \rfloor$. The channel we have identified can be characterized as a binary symmetric channel (BSC_p), which is parameterized by the probability p that an error is introduced in each bit. More formally, if Y is the output of the channel and X is the input, $\Pr[Y = b | X = 1 - b] = p$ for $b \in \{0, 1\}$. The *capacity* for BSC_p—which is the highest possible rate we could hope to achieve—is $1 - H_2(p)$ where $H_2(x) = -(x \cdot \log_2(x) + (1 - x) \cdot \log_2(1 - x))$.

Error correcting for binary channels. When we quantize the image into u different difference regions, the result is that our communication channel is actually the concatenation of u channels $Ch_1, \ldots Ch_u$. We assume that each channel Ch_i functions as a binary symmetric channel BSC_{p_i} for some probability $p_i \in [0, 1]$. Our goal is to come up with an algorithm so that, given block lengths $N_1, \ldots N_u$, we identify u codes $\mathsf{ECC}_1, \ldots \mathsf{ECC}_u$ such that $\forall j \in [u]$ (1) ECC_j can recover from errors induced by a BSC_{p_i} channel with all but low probability, (2) ECC_j has as high a rate as possible, (3) ECC_j has a practically efficient encoder and decoder, (4) ECC_j has an an alphabet size of 2^8. Requirement (4) is not actually a pure necessity, but ease implementation.

A good approach to binary codes is using a linear *concatenated code* [For65]. A linear concatenated code $\mathsf{ECC}_{out} \circ \mathsf{ECC}_{in}$ uses two codes in tandem, where messages are first using ECC_{out} and then each resulting symbol is encoded using ECC_{in}. To be precise, let the *outer code* ECC_{out} be an $[N, k, d]_Q$ where $Q = q^{k'}$ for some $k' \in \mathbb{Z}^+$ and the *inner code* ECC_{in} an $[N', k', d']_q$ code. To encode a message $\vec{m} \in \mathbb{F}_q^k$, first produce $\bar{c} = (\bar{c}_1, \ldots \bar{c}_N) = \mathsf{ECC}_{out}.\mathsf{Encode}(\vec{m})$; the final codeword is $\mathsf{ECC}_{in}.\mathsf{Encode}(\bar{c}_1), \ldots \mathsf{ECC}_{in}.\mathsf{Encode}(\bar{c}_N)$. The resulting concatenated code is an $[NN', kk', z]$ linear code where $z \geq dd'$. For binary concatenated codes, we set $q = 2$.

One approach to finding a binary concatenated codes with rate approaching capacity, involves fixing an outer code achieving the singleton bound (i.e., Reed-Solomon) and searching (via brute-force) to find a smaller inner code meeting capacity on the BSC_p channel [GRS12]. The resulting concatenated code decoder uses a maximum likelihood decoder for $\mathsf{ECC}_{in}.\mathsf{Recover}$ and then applies an efficient unique decoding algorithm for $\mathsf{ECC}_{out}.\mathsf{Recover}$. While this would produce high quality codes, it is not computationally feasible to find such an inner code probabilistically and finding "optimal" codes is beyond the scope of establishing the feasibility of our approach[5]. As such, we take a more computationally realistic approach in this work: for a given channel BSC_{p_i}, we instead do manual search over two different families of inner codes—Reed-Muller and Hamming codes—meeting our requirements from the preceding paragraph[6]. For each code, we empirically test its performance on the BSC_{p_i} for 1,000 inputs to get an accurate error rate for decoding. Consider the random variable X_ℓ to be the number of errors that occur when ℓ randomly chosen messages m_j are decoded after being put through the channel BSC_{p_i}. For a given outer code block length N, we then find the minimum $z \in \{0, \ldots, N\}$ so that $\Pr(X_N \leq z) \geq 0.99$. We then set the outer code's distance and dimension to allow recovery of up to z errors and consider only those valid codes achieving the best possible rate[7]. The full code for doing this was implemented in SageMath. See Appendix A for the list of codes we identified for Pulsar.

6 Implementation and Evaluation

We implemented Pulsar using PyTorch and the `diffusers` library [Hug] using the DDIM scheduler [SME20]. We use SageMath [The23] to provide error correcting codes. To ensure that both the sender and receiver have synchronized states, we use HMAC-DRBG [BK15] to seed our random number generators. We will release our code and benchmarks as artifacts for the community upon publication.

Our implementation uses the following diffusion models (which generate the following images): `church` (churches and other places of worship), `celebahq` (celebrity faces), `bedroom` (bedrooms), `cat` (cats), all of which were published by Google on Hugging Face [Good, Gooc, Gooa, Goob]. Example images generated by each model can be found in Appendix B.

We run our implementation on (1) "Desktop", a desktop tower with an AMD Ryzen 9 3900X CPU, NVIDIA GeForce RTX 4070 Ti GPU, and 32 GiB of RAM running Arch Linux, and (2) "Laptop", a MacBook Pro with an M1 Pro system-on-chip with 16 GiB of RAM running macOS Ventura. We believe the Laptop benchmarks are more representative of consumer hardware.

6.1 Parameter Selection

In Section 5.2, we discussed our optimized EstimateRate approach that variably encodes using different error correcting codes based on the available entropy in the image, and in Section 5.3, we discussed how we determined the library of codes to support this approach. There are two parameters in EstimateRate that we

[5] As a direction for future work, we could feasibly use Forney codes. This is theoretically more optimum except practical decoding time could drastically increase with these codes as one approaches capacity.

[6] Note, the inner code does not necessarily need a decoder that is efficient in its block length, just in the block length of the concatenated code.

[7] This means setting $d \approx 2z$ and calculating k based on d and N.

Buckets	Estimation Time (sec)	Message Length (bytes)
25	$\bar{x} = 2.84$, $s = 0.04$	$\bar{x} = 443.09$, $s = 165.58$
50	$\bar{x} = 3.08$, $s = 0.04$	$\bar{x} = 502.77$, $s = 174.44$
100	$\bar{x} = 3.10$, $s = 0.04$	$\bar{x} = 542.13$, $s = 192.75$
125	$\bar{x} = 3.10$, $s = 0.04$	$\bar{x} = 542.15$, $s = 196.67$
150	$\bar{x} = 3.11$, $s = 0.04$	$\bar{x} = 533.41$, $s = 192.61$

(a) Averages from 100 trials of our u experiment.

Estimates	Estimation Time (sec)	Success Rate
1	$\bar{x} = 2.86$, $s = 0.00$	96.0%
3	$\bar{x} = 3.79$, $s = 0.01$	93.0%
5	$\bar{x} = 4.49$, $s = 0.01$	93.0%
10	$\bar{x} = 6.22$, $s = 0.02$	87.0%
30	$\bar{x} = 13.17$, $s = 0.06$	95.0%

(b) Averages from 100 trials of our l experiment.

Model	$\bar{x}$	s	Rate	Throughput
`church`	541.70	190.82	94.0%	$E[X] = 509.20$
`celebahq`	351.02	89.04	98.0%	$E[X] = 344.00$
`bedroom`	275.00	112.70	95.0%	$E[X] = 261.25$
`cat`	386.32	288.52	98.0%	$E[X] = 378.59$

(c) Bytes encoded per-image for all models for 100 runs.

Table 1: Experimental results showing impact of u and l and the performance of different models.

have yet to determine: the number of buckets to generate for our difference regions u, and the total number of estimates to generate l. We experimentally determine these parameters for our Pulsar implementation.

Number of buckets in each estimate u. We first want to find the appropriate number of buckets to define difference regions in EstimateRate. We can increase the number of buckets to get more granular regions, but this increases execution time and may result in over-fitting. So, we fixed $l = 1$ and ran 100 iterations of EstimateRate on Desktop for multiple candidate u values on the `church` model. Our results can be found in Table 1a. $u = 100$ appears to be the best balance between mean message length, variability of the message length, and estimation time, so we choose that as the parameter.

Number of estimates l. The other parameter is the number of estimates generated during EstimateRate. We want to know if increasing *offline* estimates improves the *online* success rate – the percentage of encoded images that can be successfully decoded. Each estimate involves an iteration of a model, so we want to ensure that these additional estimates are worth the longer computation. In each trial, we fix $u = 100$ (based on our evaluation for u above), and run EstimateRate , varying l. We then encode a message using the estimated regions and see if the generated image decodes back into the same message. This shows if more estimates lead to a better chance of a successful encoding. We run 100 of these trials on Desktop and the `church` model, and show our results in Table 1b. Interestingly, our results demonstrate that additional estimates do not meaningfully improve the success probability of encoding. So, we use $l = 1$ for the remainder of this evaluation.

6.2 End-to-End Benchmarks

We run 100 trials of our implemented Pulsar system from end to end for each of the models we consider. In each trial, we run the offline step of EstimateRate, encode a random message at the sender into a 16-bit PNG image, and decode this image back into the original message. Note that we implement and provide results for the offline step of Algorithm 3; since Algorithm 2's offline step is a subset of that of Algorithm 3, we can use the same offline state for both encoding and decoding. We run our experiments on both Desktop and Laptop.

Throughput. We first seek to understand the throughput: the number of bytes per image that can be communicated steganographically with Pulsar. Table 1c summarizes this information, with information about the mean $\bar{x}$ and standard deviation s of the bytes encoded in each image, along with the rate at which the receiver can successfully decode a message. As mentioned above, decoding can fail if the estimate is not representative of the actual message encoding. The expected throughput is therefore this decoding success rate times the mean bytes per image $\bar{x}$. While the success rate is not 100%, we do note that it is high enough

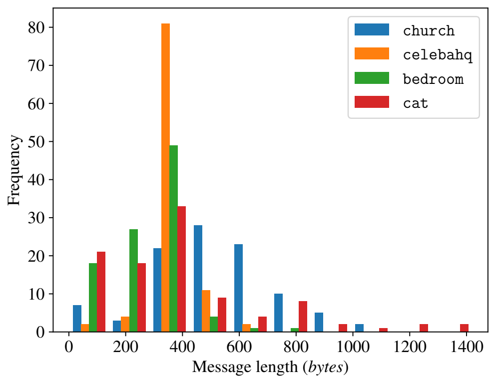

(a) The distribution of message lengths in 100 images generated for each of the models used in Pulsar.

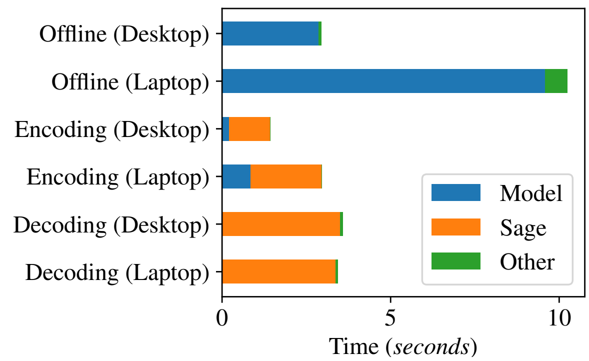

(b) The mean time spent to perform Pulsar tasks for the `church` model on Desktop and Laptop.

to support throughputs in the hundreds of bytes. Moreover, because Pulsar is a symmetric key scheme, the sender will *know* when decoding will fail and can abort.

We also seek to understand how the number of bytes per image varies between the models. We chart the distributions for this value for each model in Figure 7a. Each model has a different distribution, which is reasonable considering that each model generates substantially different images. For example, note that `celebahq` is mostly tightly centered, likely because human faces have a core structure that does not deviate significantly. On the other hand, `cat` has high variance, which we attribute to the model's lower quality (see Appendix B).

Time. Table 2 contains runtime for each phase of Pulsar for each model on both Desktop and Laptop. The offline phase is about the same for every model, which is in line with how diffusion models work. Even though each model generates different images, all models have the same number of steps (and therefore PyTorch calls to their weights), and should have the same runtimes. We see that decoding is generally slower than encoding. We can also see that the runtime of Laptop is about three times that of Desktop, and that encoding and decoding times vary between the models. In particular, the encoding and decoding times are proportional to the number of bytes the model generates (see Table 1c).

To investigate these results more, we separate each runtime by the constituent parts of Pulsar, and chart it in Figure 7b. "Model" is time spent generating an image using diffusion in PyTorch, "Sage" is time spent in SageMath's error correcting code routines, and "Other" is time spent outside of the prior two tasks. The offline phase is dominated by the model, as it is generating the estimate that will be used for the online phases. Laptop's slower runtime can thus be attributed to its lack of model processing ability relative to Desktop.

Encoding and decoding are instead dominated by SageMath. So, models that require more calls to SageMath are slower in encoding and decoding; the models that call SageMath more are those with a higher capacity for encoding bytes. For example, the `church` model takes the most time to encode/decode because it needs to encode/decode more bytes. Thus, our results are consistent. As an aside, our implementation performs a call to SageMath as a subprocess, which means our runtimes include a relatively lengthy start-up for the SageMath interpreter. A more efficient implementation (i.e., a direct implementation of the underlying ECCs without SageMath) can help reduce this runtime further.

Comparison to text model methods. We now compare our results to that of prior work on text-based steganography. We specifically compare Pulsar to [DCW+23], where the authors provide seconds per bit results for their construction, as well as those of other modern baselines such as Meteor [KJGR21]. Their hardware configuration is similar to our Desktop one.

Based on the evaluation in Table II of [DCW+23], the Pulsar construction represents a performance

Model	Desktop			Laptop		
	Offline	Encoding	Decoding	Offline	Encoding	Decoding
`church`	$\bar{x} = 2.94$, $s = 0.01$	$\bar{x} = 1.43$, $s = 0.08$	$\bar{x} = 3.58$, $s = 0.87$	$\bar{x} = 10.25$, $s = 0.16$	$\bar{x} = 2.97$, $s = 0.43$	$\bar{x} = 3.44$, $s = 0.58$
`celebahq`	$\bar{x} = 2.94$, $s = 0.01$	$\bar{x} = 1.36$, $s = 0.05$	$\bar{x} = 2.84$, $s = 0.41$	$\bar{x} = 10.25$, $s = 0.14$	$\bar{x} = 2.88$, $s = 0.21$	$\bar{x} = 2.99$, $s = 0.32$
`bedroom`	$\bar{x} = 2.94$, $s = 0.01$	$\bar{x} = 1.31$, $s = 0.08$	$\bar{x} = 2.47$, $s = 0.58$	$\bar{x} = 10.25$, $s = 0.11$	$\bar{x} = 2.84$, $s = 0.31$	$\bar{x} = 2.81$, $s = 0.42$
`cat`	$\bar{x} = 2.94$, $s = 0.01$	$\bar{x} = 1.35$, $s = 0.12$	$\bar{x} = 2.92$, $s = 1.16$	$\bar{x} = 10.24$, $s = 0.10$	$\bar{x} = 2.85$, $s = 0.24$	$\bar{x} = 3.04$, $s = 0.72$

Table 2: Average execution time for offline, encoding, and decoding steps on Desktop and Laptop for all models for 100 runs.

improvement over prior work. Using the numbers in Tables 1c and 2, the `church` model takes 1.01×10^{-3} seconds per bit to perform both the offline and encode steps, which is about twice as fast as the fastest numbers of the text-based models. Even our *Laptop* configuration is relatively performant, with 3.05×10^{-3} seconds per bit, which is similar to Discop and Meteor on *Desktop*.

We do not claim that our solution is strictly better. Text-based solutions have high utilization of the available entropy in the channel, which means that it can efficiently send smaller messages in a few hundred words. Pulsar has much lower utilization due to the noisiness of the channel. Once the messages are in the hundreds of bytes, though, Discop and related work require several paragraphs of text to encode. Pulsar instead sends an image, which, while strictly larger in file size, may be more acceptable in a channel than pages of text. With this in mind, we recommend text-based steganography for short messages, and image-based steganography for long messages.

7 Better Steganography for Diffusion Models

While Pulsar is able to encode significant amounts of information into the images generated by diffusion models, we are limited by the structure of the current generation of diffusion models. The result is that there remains capacity within these images on which we are unable to capitalize. In order to argue cryptographic security, we must adhere to the structure of existing models—changing the structure would mean that an adversary might distinguish between an image generated by our refined model and the one used more generally. We note, however, that the empirical nature of modern machine learning model development means that the structural choices within existing models are not inherent; *future* iterations of the diffusion model paradigm may both have better generative performance (when measured according to the metrics used within the machine learning literature) while also increasing the resulting image's steganographic capacity.

In this section, we highlight several ways models could be changed in order to admit higher capacity steganography. At heart, each of these changes is a way in which randomness recovery could be made easier. Importantly, these changes should not be integrated simply because they make models steganography friendly—if they result in worse model performance, the *quality* of the steganography will also suffer. Instead, we hope they can be explored as "win-win" opportunities, in which steganographic performance can be improved and model performance either improves or stays consistent.

Randomized final scheduler step. Pulsar encodes information in the second-to-last step of the scheduler since the final step is deterministic. Adding the randomness, however, is followed by another iteration of the model being applied, which perturbs the encoded information and introduces errors into the encoding. In Pulsar, we solve this through the use of error correcting codes. If the final scheduler step were randomized, we could use the same techniques developed in Pulsar to encode at the final step instead. Because there would be no additional model iteration to apply after encoding, the decoding process would be less error prone. This lack of errors would in turn allow for smaller (or even no) error correcting codes, resulting in higher utilization of the image.

Another consequence of having a deterministic final scheduler step is that we are only able to use one color channel in the generated image. Applications of the model propagates changes from one color channel to the others. In our experiments, we found that any information embedded into the variance noise of a second channel is effectively wiped out when the model is applied. As such, two thirds of the image is unusable; if the final step of the scheduler were randomized, we could theoretically triple our throughput.

Reversible model iterations. Instead of introducing randomness to the final scheduler iteration, it would also be sufficient to design model iterations that are *invertible*. That is, given access to the final image, it would be possible to recover intermediary states of the model or even the initial Gaussian noise that form the seed for the diffusion model. As discussed in Section 3.2, this seed is an excellent source of entropy that could be leveraged for steganographic embedding, but current model structures prevent the receiver from recovering the seed efficiently. Each model iteration applid to the seed modifies the image and each step is not efficiently reversible due to the nature of the neural network model.

Recovering the initialization seed would require non-trivial changes to the diffusion model structure. The internal model structures would have to change to be reversible. We note that non-linearity within the model will always make inversion more difficult, and it may be that highly non-linear models are inherent in designing performant models. Alternatively, model designers could train *pairs* of models that are able to both generate images (forwards) and recover seeds (backwards). If designing models with this property were possible, we could apply Pulsar's embedding strategy to the seed directly. In this case we would have (ideally) $n \times n \times 3$ bits of information for encoding per image, exceeding our current results (Table 1c).

Detailed and contextually appropriate models. Pulsar is best able to encode information images that are highly detailed. For example, both Figures 3d and 6a are *realistic* images of human faces. As the respective difference heatmaps in Figures 3c and 6b show, however, Figure 3d is more *detailed* (e.g., at the top of the head), which means it can encode more information in Pulsar, and is therefore a better target for encoding than Figure 6a. As such, having access to models that produced highly detailed images is desirable.

We note that there is a distinction between "detailed" and "realistic", and, of course, the quality of the generated images is critical. For instance, `cat` is a detailed model, but its relatively low quality images (see Appendix B) may make censors more suspicious. Moreover, the number of bytes it can encode has high variance, as seen in Figure 7a. Thus, future models need to prioritize detail, but not at the lack of quality.

Having models that produce images that are contextually appropriate is also critical. Our running examples in this work come from `celebahq` as they have the highest level of realism, but the model's outputs are heavily biased towards generating white, conventionally attractive faces, reflecting the biases of its training set. As a result, the images have limited contexts in which they would be appropriate. Future diffusion models should be trained on more diverse data sets. The problem of bias in model outputs is not unique to our use case, but only having a few types of outputs would be detrimental to Pulsar's real-world deployment. A censor monitoring a channel may expect only certain types of images, and perhaps images like `celebahq` or `church` would be considered strange at best, or subversive at worst. More diverse models would allow users to generate the correct types of images needed for steganography without arousing a censor's suspicion.

Support latent diffusion architectures. The models for our Pulsar evaluation are all *pixel* diffusion models, in which each model iteration performs operations on all pixels of the output image at once. Our models operate over tensors of shape $256 \times 256 \times 3$ to generate an image of dimension 256×256 with 3 color channels. As mentioned in Section 3.1, an alternative to this approach are *latent* diffusion models like Stable Diffusion [RBL+22]. Operations are performed on latents, which are a smaller representation of the image, and upscaled at the end using a VAE. Latent diffusion architectures have good results, even on relatively limited hardware.

While the core embedding strategy of Pulsar can be applied to latent diffusion models, there are barriers to making this approach productive. One is the space for encoding. The latent space used by these models typically have shape $64 \times 64 \times 3$, much smaller than that of the pixel diffusion models from our Pulsar implementation and potentially reducing throughput.

The more concerning issue is the VAE itself. Our experiments found that the VAE made it extraordinarily difficult for a receiver to determine anything about how noise was injected during model generation. In particular, because the VAE "decompresses" the latent space, applying noise to even a single element of the latent would result in noticeable changes in *many* pixels. As such, a receiver has a hard time differentiating between the effects of two neighboring latents (i.e., the effects contaminate each other). We found that encoding was possible if we spread out the locations in the latents into which we steganographically encoded, but the result *extraordinarily low* performance, e.g., 16 or 32 bits per image.

Existing approaches to VAE inversion involve estimation, and the result is not guaranteed to be the original input. Our preliminary experiments showed that attempts to reverse the VAE step resulted in too many errors to accurately reconstruct that original latents. If it were possible to design a VAE that is deterministically invertible, it would be possible to encode with very high rate into the latent space. Future work in this space could identify ways to recover latents from an image.

8 Conclusion

We present Pulsar, the first provably secure steganography scheme with support for diffusion models. Pulsar is practical, encoding hundreds of bytes per image at speeds exceeding that of prior, text-based solutions. Future work in both steganography and diffusion models can use the lessons from the design of Pulsar to create even more efficient systems.

Acknowledgments

This work was funded, in part, by the National Science Foundation's Convergence Accelerator Program, Track G under contract number 49100422C0024. The first author would like to acknowledge support from the National Science Foundation under Grant #1955172. The second author was supported by DARPA under Contract No. HR001120C0084. The third author is supported by the NSF under Grant #2030859 to the Computing Research Association for the CIFellows Project and is supported by DARPA under Agreement No. HR00112020021. Any opinions, findings and conclusions or recommendations expressed in this material are those of the author(s) and do not necessarily reflect the views of the United States Government, NSF, or DARPA.

References

[AP98] Ross J Anderson and Fabien AP Petitcolas. On the limits of steganography. *IEEE Journal on selected areas in communications*, 16(4):474–481, 1998.

[Bal17] Shumeet Baluja. Hiding images in plain sight: Deep steganography. In *Neural Information Processing Systems*, 2017.

[BC05] Michael Backes and Christian Cachin. Public-key steganography with active attacks. In Joe Kilian, editor, *TCC 2005*, volume 3378 of *LNCS*, pages 210–226. Springer, Heidelberg, February 2005.

[BK15] Elaine Barker and John Kelsey. Nist special publication 800-90a revision 1 recommendation for random number generation using deterministic random bit generators, 2015.

[BM82] Manuel Blum and Silvio Micali. How to generate cryptographically strong sequences of pseudo random bits. In *23rd FOCS*, pages 112–117. IEEE Computer Society Press, November 1982.

[Cac00] Christian Cachin. An information-theoretic model for steganography. Cryptology ePrint Archive, Report 2000/028, 2000. https://eprint.iacr.org/2000/028.

[CC10] Ching-Yun Chang and Stephen Clark. Linguistic steganography using automatically generated paraphrases. In *Human Language Technologies: The 2010 Annual Conference of the North American Chapter of the Association for Computational Linguistics*, HLT '10, pages 591–599, Stroudsburg, PA, USA, 2010. Association for Computational Linguistics.

[CC14] Ching-Yun Chang and Stephen Clark. Practical linguistic steganography using contextual synonym substitution and a novel vertex coding method. *Computational Linguistics*, 40(2):403–448, Jun 2014.

[Cha19] Marc Chaumont. Deep learning in steganography and steganalysis from 2015 to 2018, 2019.

[DC19] Falcon Dai and Zheng Cai. Towards near-imperceptible steganographic text. *Proceedings of the 57th Annual Meeting of the Association for Computational Linguistics*, 2019.

[DCRS13] Kevin P. Dyer, Scott E. Coull, Thomas Ristenpart, and Thomas Shrimpton. Protocol misidentification made easy with format-transforming encryption. In Ahmad-Reza Sadeghi, Virgil D. Gligor, and Moti Yung, editors, *ACM CCS 2013*, pages 61–72. ACM Press, November 2013.

[DCS15] Kevin P. Dyer, Scott E. Coull, and Thomas Shrimpton. Marionette: A programmable network traffic obfuscation system. In *24th USENIX Security Symposium (USENIX Security 15)*, pages 367–382, Washington, D.C., 2015. USENIX Association.

[DCW+23] J. Ding, K. Chen, Y. Wang, N. Zhao, W. Zhang, and N. Yu. Discop: Provably secure steganography in practice based on "distribution copies". In *2023 IEEE Symposium on Security and Privacy (SP)*, pages 2238–2255, Los Alamitos, CA, USA, may 2023. IEEE Computer Society.

[DMS04] Roger Dingledine, Nick Mathewson, and Paul Syverson. Tor: The second-generation onion router. In *Proceedings of the 13th Conference on USENIX Security Symposium - Volume 13*, SSYM'04, pages 21–21, Berkeley, CA, USA, 2004. USENIX Association.

[DN21] Prafulla Dhariwal and Alexander Nichol. Diffusion models beat gans on image synthesis. *Advances in neural information processing systems*, 34:8780–8794, 2021.

[FJA17] Tina Fang, Martin Jaggi, and Katerina Argyraki. Generating steganographic text with lstms. *Proceedings of ACL 2017, Student Research Workshop*, 2017.

[FLH+15] David Fifield, Chang Lan, Rod Hynes, Percy Wegmann, and Vern Paxson. Blocking-resistant communication through domain fronting. *Proceedings on Privacy Enhancing Technologies*, 2015(2):46–64, 2015.

[For65] G David Forney. Concatenated codes. 1965.

[FPK07] Jessica Fridrich, Tomáš Pevný, and Jan Kodovský. Statistically undetectable jpeg steganography: Dead ends challenges, and opportunities. In *Proceedings of the 9th Workshop on Multimedia & Security*, MM&Sec '07, page 3–14, New York, NY, USA, 2007. Association for Computing Machinery.

[GGA+05] Christian Grothoff, Krista Grothoff, Ludmila Alkhutova, Ryan Stutsman, and Mikhail Atallah. Translation-based steganography. In *International Workshop on Information Hiding*, pages 219–233. Springer, 2005.

[Gooa] Google. ddpm-bedroom-256. https://huggingface.co/google/ddpm-bedroom-256.

[Goob] Google. ddpm-cat-256. https://huggingface.co/google/ddpm-cat-256.

[Gooc] Google. ddpm-celebahq-256. https://huggingface.co/google/ddpm-celebahq-256.

[Good] Google. ddpm-church-256. https://huggingface.co/google/ddpm-church-256.

[GRS12] Venkatesan Guruswami, Atri Rudra, and Madhu Sudan. Essential coding theory. *Draft available at http://www. cse. buffalo. edu/atri/courses/coding-theory/book*, 2(1), 2012.

[Har18] Harveyslash. harveyslash/deep-steganography. https://github.com/harveyslash/Deep-Steganography, Apr 2018.

[HH19] SHIH-YU HUANG and Ping-Sheng Huang. A homophone-based chinese text steganography scheme for chatting applications. *Journal of Information Science & Engineering*, 35(4), 2019.

[HJA20] Jonathan Ho, Ajay Jain, and Pieter Abbeel. Denoising diffusion probabilistic models. *Advances in neural information processing systems*, 33:6840–6851, 2020.

[HLv02] Nicholas J. Hopper, John Langford, and Luis von Ahn. Provably secure steganography. In Moti Yung, editor, *CRYPTO 2002*, volume 2442 of *LNCS*, pages 77–92. Springer, Heidelberg, August 2002.

[HPRV19] Thibaut Horel, Sunoo Park, Silas Richelson, and Vinod Vaikuntanathan. How to subvert backdoored encryption: Security against adversaries that decrypt all ciphertexts. In Avrim Blum, editor, *ITCS 2019*, volume 124, pages 42:1–42:20. LIPIcs, January 2019.

[HRBS13] Amir Houmansadr, Thomas J. Riedl, Nikita Borisov, and Andrew C. Singer. I want my voice to be heard: IP over voice-over-IP for unobservable censorship circumvention. In *NDSS 2013*. The Internet Society, February 2013.

[Hug] Hugging Face. diffusers. https://github.com/huggingface/diffusers.

[HWJ+18] D. Hu, L. Wang, W. Jiang, S. Zheng, and B. Li. A novel image steganography method via deep convolutional generative adversarial networks. *IEEE Access*, 6:38303–38314, 2018.

[KJGR21] Gabriel Kaptchuk, Tushar M. Jois, Matthew Green, and Aviel D. Rubin. Meteor: Cryptographically secure steganography for realistic distributions. In Giovanni Vigna and Elaine Shi, editors, *ACM CCS 2021*, pages 1529–1548. ACM Press, November 2021.

[Kor23] Jennifer Korn. Microsoft outlook will soon write emails for you. CNN, 10 2023.

[KW13] Diederik P Kingma and Max Welling. Auto-encoding variational bayes. *arXiv preprint arXiv:1312.6114*, 2013.

[LDJ+14] Daniel Luchaup, Kevin P. Dyer, Somesh Jha, Thomas Ristenpart, and Thomas Shrimpton. Libfte: A toolkit for constructing practical, format-abiding encryption schemes. In *23rd USENIX Security Symposium (USENIX Security 14)*, pages 877–891, San Diego, CA, 2014. USENIX Association.

[Le03] Tri Van Le. Efficient provably secure public key steganography. Cryptology ePrint Archive, Report 2003/156, 2003. https://eprint.iacr.org/2003/156.

[LK03] Tri Van Le and Kaoru Kurosawa. Efficient public key steganography secure against adaptively chosen stegotext attacks. Cryptology ePrint Archive, Report 2003/244, 2003. https://eprint.iacr.org/2003/244.

[Mit99] Thomas Mittelholzer. An information-theoretic approach to steganography and watermarking. In *International Workshop on Information Hiding*, pages 1–16. Springer, 1999.

[MLDG12] Hooman Mohajeri Moghaddam, Baiyu Li, Mohammad Derakhshani, and Ian Goldberg. SkypeMorph: protocol obfuscation for Tor bridges. In Ting Yu, George Danezis, and Virgil D. Gligor, editors, *ACM CCS 2012*, pages 97–108. ACM Press, October 2012.

[OYZ+20] Jonathan Oakley, Lu Yu, Xingsi Zhong, Ganesh Kumar Venayagamoorthy, and Richard Brooks. Protocol proxy: An fte-based covert channel. *Computers & Security*, 92:101777, May 2020.

[PM] Trevor Perrin and Moxie Marlinspike. he double ratchet algorithm. Available at https://whispersystems.org/docs/specifications/doubleratchet/.

[PPY22] Giuseppe Persiano, Duong Hieu Phan, and Moti Yung. Anamorphic encryption: Private communication against a dictator. In Orr Dunkelman and Stefan Dziembowski, editors, *EUROCRYPT 2022, Part II*, volume 13276 of *LNCS*, pages 34–63. Springer, Heidelberg, May / June 2022.

[RBL+22] Robin Rombach, Andreas Blattmann, Dominik Lorenz, Patrick Esser, and Björn Ommer. High-resolution image synthesis with latent diffusion models. In *Proceedings of the IEEE/CVF conference on computer vision and pattern recognition*, pages 10684–10695, 2022.

[Res18] Eric Rescorla. Rfc 8446 - the transport layer security (tls) protocol version 1.3. https://datatracker.ietf.org/doc/html/rfc8446#page-160, 2018.

[RR03] Leonid Reyzin and Scott Russell. Simple stateless steganography. Cryptology ePrint Archive, Report 2003/093, 2003. https://eprint.iacr.org/2003/093.

[RSG98] M. G. Reed, P. F. Syverson, and D. M. Goldschlag. Anonymous connections and onion routing. *IEEE Journal on Selected Areas in Communications*, 16(4):482–494, May 1998.

[Ruh17] Sylvain Ruhault. SoK: Security models for pseudo-random number generators. *IACR Trans. Symm. Cryptol.*, 2017(1):506–544, 2017.

[SAZ+18] Ayon Sen, Scott Alfeld, Xuezhou Zhang, Ara Vartanian, Yuzhe Ma, and Xiaojin Zhu. Training set camouflage. *Decision and Game Theory for Security*, page 59–79, 2018.

[SCC07] Yun Q Shi, Chunhua Chen, and Wen Chen. A markov process based approach to effective attacking jpeg steganography. In *Information Hiding: 8th International Workshop, IH 2006, Alexandria, VA, USA, July 10-12, 2006. Revised Selcted Papers 8*, pages 249–264. Springer, 2007.

[SDWMG15] Jascha Sohl-Dickstein, Eric Weiss, Niru Maheswaranathan, and Surya Ganguli. Deep unsupervised learning using nonequilibrium thermodynamics. In *International conference on machine learning*, pages 2256–2265. PMLR, 2015.

[Sim83] Gustavus J. Simmons. The prisoners' problem and the subliminal channel. In David Chaum, editor, *CRYPTO'83*, pages 51–67. Plenum Press, New York, USA, 1983.

[SME20] Jiaming Song, Chenlin Meng, and Stefano Ermon. Denoising diffusion implicit models. *arXiv preprint arXiv:2010.02502*, 2020.

[SSM+06a] K. Solanki, K. Sullivan, U. Madhow, B. S. Manjunath, and S. Chandrasekaran. Provably secure steganography: Achieving zero k-l divergence using statistical restoration. In *2006 International Conference on Image Processing*, pages 125–128, Oct 2006.

[SSM+06b] Kenneth Sullivan, Kaushal Solanki, B. S. Manjunath, Upamanyu Madhow, and Shivkumar Chandrasekaran. Determining achievable rates for secure, zero divergence, steganography. In *ICIP*, pages 121–124. IEEE, 2006.

[SSM07] A. Sarkar, K. Solanki, and B. S. Manjunath. Secure steganography: Statistical restoration in the transform domain with best integer perturbations to pixel values. In *IEEE International Conference on Image Processing (ICIP)*, Sep 2007.

[SSSS07] Mohammad Shirali-Shahreza and M. H. Shirali-Shahreza. Text steganography in sms. *2007 International Conference on Convergence Information Technology (ICCIT 2007)*, pages 2260–2265, 2007.

[The23] The Sage Developers. *SageMath, the Sage Mathematics Software System (Version x.y.z)*, 2023. https://www.sagemath.org.

[Tor] Tor Project. The tor project: Privacy and freedom online. https://www.torproject.org/.

[vH04] Luis von Ahn and Nicholas J. Hopper. Public-key steganography. In Christian Cachin and Jan Camenisch, editors, *EUROCRYPT 2004*, volume 3027 of *LNCS*, pages 323–341. Springer, Heidelberg, May 2004.

[Vin22] James Vincent. Ai-generated selfies could be the next snapchat filters. The Verge, 10 2022.

[VNBB17] Denis Volkhonskiy, Ivan Nazarov, Boris Borisenko, and Evgeny Burnaev. Steganographic generative adversarial networks, 2017.

[WGN+12] Qiyan Wang, Xun Gong, Giang T. K. Nguyen, Amir Houmansadr, and Nikita Borisov. CensorSpoofer: asymmetric communication using IP spoofing for censorship-resistant web browsing. In Ting Yu, George Danezis, and Virgil D. Gligor, editors, *ACM CCS 2012*, pages 121–132. ACM Press, October 2012.

[Wha17] WhatsApp. WhatsApp Encryption Overview. Available at https://scontent.whatsapp.net/v/t61/68135620_760356657751682_6212997528851833559_n.pdf/WhatsApp-Security-Whitepaper.pdf, December 2017.

[WPF13] Philipp Winter, Tobias Pulls, and Jürgen Fuß. Scramblesuit: A polymorph network protocol to circumvent censorship. *CoRR*, abs/1305.3199, 2013.

[WYL18] Pin Wu, Yang Yang, and Xiaoqiang Li. Stegnet: Mega image steganography capacity with deep convolutional network. *Future Internet*, 10(6):54, Jun 2018.

[Xia18] Lingyun Xiang. Reversible natural language watermarking using synonym substitution and arithmetic coding, 2018.

[YGC+19] Z. Yang, X. Guo, Z. Chen, Y. Huang, and Y. Zhang. Rnn-stega: Linguistic steganography based on recurrent neural networks. *IEEE Transactions on Information Forensics and Security*, 14(5):1280–1295, May 2019.

[YHC+09] Zhenshan Yu, Liusheng Huang, Zhili Chen, Lingjun Li, Xinxin Zhao, and Youwen Zhu. Steganalysis of synonym-substitution based natural language watermarking, 2009.

[YJH+18] Zhongliang Yang, Shuyu Jin, Yongfeng Huang, Yujin Zhang, and Hui Li. Automatically generate steganographic text based on markov model and huffman coding, 2018.

[ZDR19] Zachary M. Ziegler, Yuntian Deng, and Alexander M. Rush. Neural linguistic steganography, 2019.

[ZFK+98] Jan Zöllner, Hannes Federrath, Herbert Klimant, Andreas Pfitzmann, Rudi Piotraschke, Andreas Westfeld, Guntram Wicke, and Gritta Wolf. Modeling the security of steganographic systems. In *International Workshop on Information Hiding*, pages 344–354. Springer, 1998.

A Additional Details on Error Correction in Pulsar

Pulsar uses error correcting codes to improve the performance of the steganographic channel inside of diffusion models. A more formal treatment description of the EstimateRate used in Pulsar can be found in Algorithm 4. Note that our optimized EstimateRate requires the estimation of the errors in the current model state by performing trial encoding and decoding of random messages. We define a subroutine in Algorithm 5, CalcErrors, that performs this estimation for EstimateRate. Note that the parameters EstimateRate is parameterized the by the number of buckets in each estimate u and l, which we discuss in Section 6.1 in the main body of this paper.

Error Rate	Outer Code	Inner Code	Input Size (*bytes*)	Output Size (*bits*)
0.05	`GeneralizedReedSolomonCode(GF(256)[:255], 200)`	`HammingCode(GF(2), 3)`	200	3570
0.10	`GeneralizedReedSolomonCode(GF(256)[:255], 100)`	`HammingCode(GF(2), 3)`	100	3570
0.15	`GeneralizedReedSolomonCode(GF(256)[:255], 220)`	`BinaryReedMullerCode(1, 5)`	220	10880
0.30	`GeneralizedReedSolomonCode(GF(256)[:255], 200)`	`BinaryReedMullerCode(1, 7)`	200	32640
0.35	`GeneralizedReedSolomonCode(GF(256)[:255], 100)`	`BinaryReedMullerCode(1, 7)`	100	32640

Table 3: The library of error correcting codes used for Pulsar.

Table 3 contains information on the concrete codes library that we built for Pulsar. We provide the exact SageMath function calls that generate our outer and inner codes. This library forms the $\mathsf{Library}_{\mathsf{ECC}}$ in Algorithm 4.

As we discovered these codes experimentally, we make no claims about optimality. In particular, note that the code for error rate 0.15 does not meet the traditional definition of a concatenated code, since there is a mismatch between the codeword size of the outer code (8 bits) and the message size of the inner code (6 bits). In our testing, however, the code performed well, and we included it in our library. We leave a more systematic design for the concrete error correcting codes used in Pulsar to future work.

Algorithm 4: Pulsar EstimateRate

Input: Model state s_{t-2}
Output: Difference region-based ECC rates rate
`// Get error rates at each pixel`
err ← CalcErrors(l)
`// Bucket regions based on error rates`
regions ← Bucketize(err, u)
for region ∈ regions **do**
  regionErr ← mean(err[region])
  `// Select appropriate ECC parameters`
  params ← $\mathsf{Library}_{\mathsf{ECC}}$[regionErr])
  rate[region] ← params
Output rate

Figure 8: The optimized EstimateRate used in Pulsar.

Algorithm 5: CalcErrors

Input: Model state s_{t-2}, Number of estimates l
Output: Mean error rates at each pixel location err
for $1 \le g < l$ **do**
    `// Similar to the online phase of encoding`
    $m \xleftarrow{\$} [0,1]^{n\times n}$
    for $0 \le j < |m|$ **do**
        if $m[j] = \mathit{0}$ **then**
            $r_{t-1}[j] \xleftarrow{\$} \mathcal{N}_{k_0}$
        else
            $r_{t-1}[j] \xleftarrow{\$} \mathcal{N}_{k_1}$
    $\mathsf{pred}_{t-1} \leftarrow \mathsf{Model}(s_{t-2})$
    $s_{t-1} \leftarrow \mathsf{Scheduler}_{t-1}(s_{t-2}, \mathsf{pred}_{t-1}; r_{t-1})$
    `// Deterministic Final Schedule`
    $\mathsf{pred}_t \leftarrow \mathsf{Model}(s_{t-1})$
    $\mathsf{img} \leftarrow \mathsf{Scheduler}_t(s_{t-1}, \mathsf{pred}_t)$
    `// Similar to the offline phase of decoding`
    `// Generate reference image 0`
    Set $r^0_{t-1} \xleftarrow{\$} \mathcal{N}^{n\times n}_{k_0}$
    Set $s^0_{t-1} \leftarrow \mathsf{Scheduler}_{t-1}(s_{t-2}, \mathsf{pred}_{t-1}; r^0_{t-1})$
    $\mathsf{pred}^0_t \leftarrow \mathsf{Model}(s^0_{t-1})$
    $\mathsf{img}_0 \leftarrow \mathsf{Scheduler}_t(s^0_{t-1}, \mathsf{pred}^0_t)$
    `// Generate reference image 1`
    $r^1_{t-1} \xleftarrow{\$} \mathcal{N}^{n\times n}_{k_1}$
    Set $s^1_{t-1} \leftarrow \mathsf{Scheduler}_{t-1}(s_{t-2}, \mathsf{pred}_{t-1}; r^1_{t-1})$
    $\mathsf{pred}^1_t \leftarrow \mathsf{Model}(s^1_{t-1})$
    $\mathsf{img}_1 \leftarrow \mathsf{Scheduler}_t(s^1_{t-1}, \mathsf{pred}^1_t)$
    `// Similar to the online phase of decoding`
    for $0 \le j < |m|$ **do**
        if $|\mathsf{img}[j] - \mathsf{img}_0[j]| < |\mathsf{img}[j] - \mathsf{img}_1[j]|$ **then**
            $m'[j] \leftarrow 0$
        else
            $m'[j] \leftarrow 1$
    `// Save the n` $\times$ `n matrix of magnitudes to a list`
    $\mathsf{errs}[g] \leftarrow \mathsf{abs}(m - m')$
`// Mean of all estimated magnitudes`
Output $\mathsf{err} \leftarrow \mathsf{mean}(\mathsf{errs})$

Figure 9: The CalcErrors subroutine of EstimateRate.

B Sample Pulsar Images

Figure 10 contains additional sample images from our Pulsar evaluation. In each figure, the first image represents the image generated by model on which Pulsar achieved the best encoding length, and the second image represents the one on which Pulsar achieved the worst encoding length.

(a) A Pulsar image from the `church` model which encodes 1120 bytes.

(b) A Pulsar image from the `church` model which encodes 100 bytes.

(c) A Pulsar image from the `bedroom` model which encodes 720 bytes.

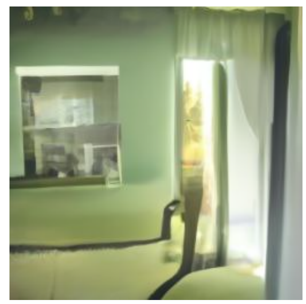

(d) A Pulsar image from the `bedroom` model which encodes 100 bytes.

(e) A Pulsar image from the `cat` model which encodes 1420 bytes.

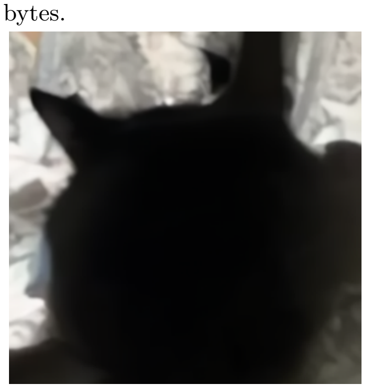

(f) A Pulsar image from the `cat` model which encodes 100 bytes.

Figure 10: Sample Pulsar outputs from the `church`, `bedroom`, and `cat` models.